International Journal of Thin Films Science and Technology

http://dx.doi.org/10.18576/ijtfst/140303

Cs Base Different Haliade (Br,I,Cl): Comparable Study Perovskits Solar Cells

Maily A. Ghali[*] *and Samir M. AbdulAlmohsin*

Department of Physics, College of Education for Pure Sciences, Thi-Qar University, Thi-Qar,64001, Iraq

Received: 2 Mar. 2025, Revised: 12 Jun. 2025, Accepted: 22 Jul. 2025
Published online: 1 Sep. 2025

Abstract: This study investigates cesium-based halide perovskite solar cells with varying halides (Br, I, Cl) to assess their impact on device performance. By comparing $CsPbBr_3$, $CsPbI_3$, and $CsPbCl_3$ compositions, the work explores their optical and structural properties using numerical simulation and available experimental data. The device architecture incorporates a graphene (Gr)-based electron transport layer (ETL) to enhance electron mobility and reduce recombination losses, while the hole transport material (HTM) layer is constructed using carbon nanotubes (CNTs) to improve hole extraction and charge transport. The results show that halide substitution significantly influences the bandgap and overall device behavior. Among the studied compositions, $CsPbI_3$ achieved the highest power conversion efficiency (PCE) (19.9), the highest short-circuit current density Jsc (24.9), and the highest fill factor FF (72.0), making it the most promising candidate for high-performance perovskite solar cells.

Keywords: Perovskite solar cell (PSC), Electron transport layer (ETL), Hole transport layer (HTL), Graphene (Gr).

1 Introduction

Perovskite solar cells (PSCs) are considered one of the most promising emerging photovoltaic technologies due to their remarkable progress in recent years. Since their initial introduction in 2009, PSCs have attracted considerable attention in both academic and industrial fields because of their excellent optoelectronic properties and low-cost fabrication processes. A number of studies have reported significant improvements in their power conversion efficiency (PCE), increasing from an initial value of 3.8% to over 25.2% within a relatively short period. Additionally, the overall cost of manufacturing PSCs has decreased compared to traditional silicon-based solar cells, making them a competitive alternative for future sustainable energy production. The fundamental structure of a perovskite material is commonly represented by the general formula ABX_3, where A and B are cations of different sizes, and X is an anion, typically a halide ion, that maintains charge neutrality. Among the different types of halide perovskites, those based on iodide have demonstrated superior electronic and optoelectronic properties. This is largely due to their higher carrier mobility, long charge carrier diffusion lengths, and strong optical absorption coefficients, all of which are essential parameters for efficient solar energy conversion. Despite their impressive properties and rapid development, PSCs face several challenges that hinder their commercial application. One of the primary issues is the instability and degradation of device performance over time, particularly under environmental stresses such as moisture, heat, and ultraviolet radiation. To enhance the stability and efficiency of PSCs, the device architecture typically involves the incorporation of additional functional layers. Specifically, the perovskite active layer is positioned between an electron transporting material (ETM) and a hole transporting material (HTM). These layers are crucial for facilitating the efficient separation and transport of photogenerated charge carriers. The ETM layer collects and transports electrons, while the HTM layer does the same for holes, minimizing recombination losses and improving the overall device performance. Numerous studies have highlighted the importance of selecting suitable ETM and HTM materials to optimize the performance and stability of PSCs [1] .[2] Furthermore, the formation of excitons—bound electron-hole pairs—within the perovskite layer, and their subsequent dissociation and transportation into respective charge transport layers, is a key process in achieving high power conversion efficiencies. In conclusion, while PSCs offer outstanding potential as next-generation photovoltaic devices due to their exceptional material properties and cost-effectiveness, ongoing research is essential to address their stability issues and optimize their structural components. This will pave the way for their practical application in the renewable energy market.

2 Theory and Modeling

The structural configuration of a typical perovskite solar cell (PSC) is depicted in Fig. 1. From the bottom up, the device is composed of a gold (Au) layer, which functions as the back contact, followed by a hole transport layer (HTL) made of p-type material. Above this is the perovskite active layer (ABX3) responsible for light absorption and charge generation. (Gr) layer serves as the electron transport layer

[*]Corresponding author E-mail: maali_abdallah@gmail.com

(ETL), which is placed underneath a fluorine-doped tin oxide (FTO) layer acting as the transparent conducting electrode (TCO). Finally, the device is exposed to air at the top surface to investigate the photovoltaic performance of the PSC, a combined optical and electrical simulation model was employed to extract essential device parameters and operational characteristics.

2.1 Optical Model

The optical analysis involves determining the distribution of the electric field, the absorption profile, and the photogeneration rate within the multilayer structure of the PSC. This is achieved by solving the Helmholtz equation, which is derived from Maxwell's equations in the frequency domain. The equation governing the propagation of the electric field within the structure is given by:

$$\frac{d^2\ E(x)}{dx^2} + \mathrm{K}_o^2\ \varepsilon_{r(x)} E(x) = 0 \qquad (1)$$

where:

E(x)is the electric field intensity at a given position, x

κ_o is the wavevector in a vacuum ($\kappa_{o=\frac{2\Pi}{\lambda_o}}$)

$\varepsilon_r(x)$represents the position-dependent relative permittivity of each material layer.

By solving this equation, the optical behavior of light within the PSC structure can be accurately predicted, enabling the calculation of the spatial distribution of photogeneration rates. These results are subsequently utilized as input for the electrical simulation to model charge transport and recombination mechanisms.

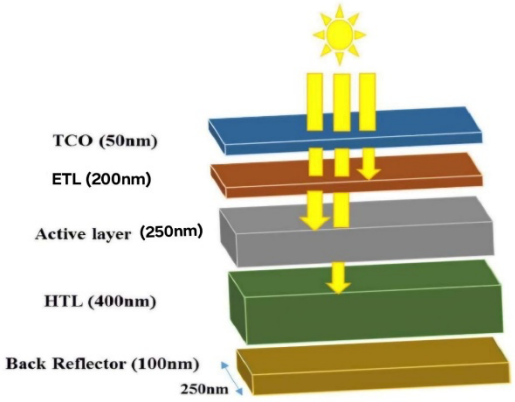

Fig. 1: The 3D schematics of PSC and the thicknesses of layers.

The relative permittivity (εr) of materials varies with the incident light wavelength (λ). To accurately simulate the propagation of electromagnetic waves within the multilayer structure, two essential optical parameters are required for each layer: the refractive index n(λ) and the extinction coefficient k(λ). The values of these optical constants for various materials — including

The distribution of the electric field intensity throughout the device structure is computed according to Equation (1):

E(λ) = calculated using Maxwell's equations and material parameters.}

Once the electric field intensity |E(λ)|² is known, the photogeneration rate G_{ph}(λ) at each wavelength is determined using the following relation:

$$G_{ph}(\lambda) = \frac{\varepsilon''(\lambda) E(\lambda)^2}{2h} \qquad (2)$$

where h is Planck's constant, and ε"(λ) represents the imaginary component of the relative permittivity at the corresponding wavelength (λ).

This calculation is performed over the visible light range, specifically from 300 nm to 800 nm, with a focus on three critical layers within the device architecture: the electron transport layer (ETL), the active absorber layer, and the hole transport layer (HTL).

For the simulation configuration, a plane wave source based on the standard AM1.5G solar spectrum is used. Floquet periodic boundary conditions (PBCs) are applied along the lateral sides of the structure to model periodicity, while the back surface — composed of a gold (Au) layer — is treated with a perfect electric conductor (PEC) boundary condition. This PEC boundary reflects unabsorbed photons, improving light trapping and internal reflection.

Finally, the total photogeneration rate is obtained by integrating G(λ) over the entire wavelength range of interest:

$$G_{ph,total} = \int_{300nm}^{800nm} G_{ph}(\lambda) d\lambda \qquad (3)$$

This approach provides a comprehensive assessment of the optical and electrical performance of the multilayer device structure under simulated solar illumination. [2], [3]

3 Electrical Mode

In this section, the distribution of charge carriers within the perovskite solar cell (PSC) is analyzed to determine its current-voltage (J-V) characteristics. To achieve this, the Poisson equation and the continuity equations for both electrons and holes are solved across the different layers of the device — including the electron transport layer (ETL), hole transport layer (HTL), and the active layer.

The electrostatic potential distribution within the device is governed by the Poisson equation:

$$\nabla.(\varepsilon_\circ \varepsilon_r \nabla \boldsymbol{\psi}) = -\boldsymbol{\rho} \qquad (4)$$

where:

$\varepsilon_\circ$is the vacuum permittivity,

$\varepsilon_r$is the relative permittivity of the material,

ψ represents the electrostatic potential,

ρ is the local charge density.

The charge density is defined as:

$$\rho = q(p - n + N_D^+ - N_A^-) \quad (5)$$

where:

n and p are the electron and hole concentrations, respectively,

N_D^+ and N_A^- represent the densities of ionized donors and acceptors.

The temporal evolution of the carrier concentrations is described by the continuity equations for electrons and holes:

$$\frac{\partial n}{\partial t} = \frac{1}{q}\nabla.J_n + G_n\text{-}U_n \quad (6)$$

$$\frac{\partial p}{\partial t} = -\frac{1}{q}\nabla.J_p + G_p\text{-}U_p \quad (7)$$

where:

$J_p$and J_n are the current densities of electrons and holes,

$G_n$and G_p are the generation rates of electrons and holes obtained from the optical analysis,

$U_p$and U_n denote the recombination rates.

The current densities are calculated using the drift-diffusion model as follows:

$$J_n = q\mu_n \mathrm{n}\nabla\boldsymbol{\psi} + \boldsymbol{qD_n}\nabla\mathbf{n} \quad (8)$$

$$J_p = -q\mu_p \mathrm{p}\,\nabla\boldsymbol{\psi} + \boldsymbol{qD_p}\nabla\mathbf{p} \quad (9)$$

where:

$\mu_n$and μ_p are the mobilities of electrons and holes,

$\boldsymbol{D_p}$and $\boldsymbol{D_n}$ are the diffusion coefficients for electrons and holes.

In this electrical model, Shockley-Read-Hall (SRH) recombination is considered the primary recombination mechanism. It is expressed by:

$$R_{SRH} = \frac{n_{p-n_i^2}}{\tau_{p\,(n+n_1)+\tau_n\,(p+p_1)}} \quad (10)$$

where:

$n_i$is the intrinsic carrier concentration,

$\tau_p$and τ_n are the carrier lifetimes for electrons and holes, respectively.

Table 1: The electrical parameters of PSC

Parameter	Cs pbI_3	Cs pbBr_3	Cs pbCl_3	Gr	CNT
Thickness (nm)	250	250	250	200	400
Permittivity (Relative), ε_r	17.6	15	10	6.9	5.5
CB density of states, Nc (1/cm3)	$10^{18} * 2.2$	$10^{18} * 2.5$	$10^{18} * 2.8$	$10^{19} * 1$	$10^{19} * 1$
VB density of states, Nv(1/cm3)	$10^{18} * 2.2$	$10^{18} * 2.5$	$10^{18} * 2.8$	$10^{19} * 1$	$10^{19} * 1$
Electron Mobility, μ_n (cm² /Vs)'	15	7	3	9000	1200
Hole Mobility, μ_h (cm² VS)	10	5	2	9000	1100
Electron affinity,ℵ(eV)	3.9	3.5	3.1	4.4	4.2
Band gap, Eg (eV)	1.73	2.3	3.0	0.1	0.2
Acceptor density, N_A(1/cm³)	$10^{13} * 1$	$10^{13} * 1$	$10^{13} * 1$	---	--
Donor density, N_D (1/ cm³	---	---	---	$10^{19} * 1$	$10^{19} * 1$
τ_n/τ_p	$\frac{8}{8}$	$\frac{5}{5}$	$\frac{5}{5}$	0.005/0.005	0.01/0.01

In perovskite solar cells (PSCs), the performance of the device is largely determined by the alignment of energy levels and the mobility of charge carriers across the different layers. Table (1.1) outlines essential electrical properties for three perovskite absorber materials ($CsPbI_3$, $CsPbBr_3$, $CsPbCl_3$) and two possible transport layers – graphene (Gr) and carbon nanotubes (CNT).

The energy band gap (E_9) of the perovskite materials increases from $CsPbI_3$ (1.73 eV) to $CsPbCl_3$ (3.0 eV), indicating a shift in optical absorption behavior. $CsPbI_3$, with the lowest band gap, absorbs a broader range of the solar spectrum, making it ideal for single-junction solar cells. In contrast, $CsPbCl_3$, with its wide band gap, is more suited for top cells in tandem architectures, where UV or high-energy photons are targeted.

When visualizing the band alignment, as shown in a schematic energy band diagram (similar to Fig. 2), the conduction band minimum (CBM) and valence band maximum (VBM) of the perovskite must be appropriately matched with the electron and hole transport layers, respectively. For effective electron transport, the CBM of the perovskite should be at a higher ievel(i.e.more negative vaiue)than the conduction band of the ETL (e.g., Gr). Graphene, with its high electron mobility (9000 cm²/Vs) and work function of ~4.4 eV, aligns well with the conduction band of the perovskite and the FTO layer. This allows photogenerated electrons in the perovskite to trans [4], [5], [6] ,and [7].

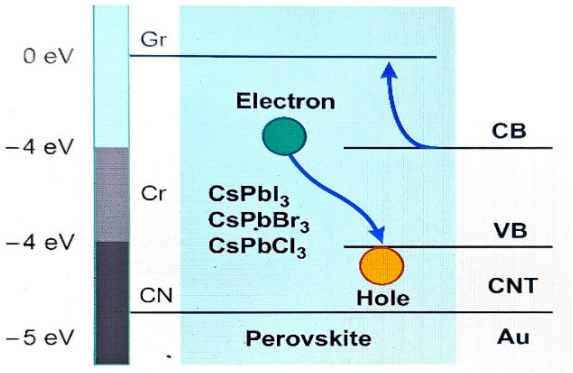

Fig. 2: The performance and layers band diagram energy levels of PSC

The performance and efficiency of perovskite solar cells (PSCs) are largely governed by the alignment of energy levels between the perovskite absorber layer and the adjacent charge transport layers. This alignment is typically described in terms of the conduction band minimum (CBM) and valence band maximum (VBM) of the perovskite material, and their relative positions to the work functions or band edges of the electron and hole transport materials.

Perovskite materials such as Cs Pb I_3, $CsPbBr_3$, and $CsPbCl_3$ serve as the light-absorbing layer, where incident photons excite electrons from the VBM to the CBM, leaving behind holes. The effective extraction of these photo-generated charge carriers depends on the energetic compatibility with adjacent layers.

In the illustrated band diagram, the energy levels of each component are depicted as follows:

The conduction band of the perovskite must be positioned above the energy level of the electron transport layer (ETL), such as graphene, to enable facile electron injection.

Similarly, the valence band must be close to or lower than the energy level (work function) of the hole transport layer (HTL), such as carbon nanotubes (CNTs), to promote efficient hole extraction.

Graphene (Gr), with a relatively low work function (~4.4 eV) and high electron mobility, is well-suited for serving as an ETL, allowing electrons to transfer efficiently from the perovskite layer to the transparent conductive oxide (FTO). On the other hand, CNTs possess a higher work function (~4.8–5.0 eV), making them suitable for hole transport, as they align favorably with the VBM of the perovskite and facilitate hole extraction toward the back electrode (e.g., Au).

This optimal band alignment minimizes energy barriers at the interfaces, reduces recombination losses, and ensures efficient charge carrier separation and transport. Consequently, such insights are critical in guiding the selection and engineering of materials for achieving high-efficiency PSCs.

Table 2: Effect of Gr Layer Thickness on Solar Cell Performance Parameters

Thickness(nm) Gr	V_{OC} (volt)	J_{SC} $(\frac{mA}{Cm^2})$	F.F (%)	η (%)
10	2.461	16.241	30.50	12.03
20	2.261	16.50	31.00	11.92
30	2.240	16.00	31.80	11.87
40	2.220	15.50	32.00	11.81
50	2.112	15.32	32.16	11.77
100	2.052	14.39	33.97	10.04
150	1.955	12.18	35.75	8.52
200	1.876	10.59	37.41	7.44
250	1.810	9.452	38.88	6.65
300	1.753	8.591	40.20	6.06
350	1.705	7.917	41.37	5.59
400	1.662	7.375	42.43	5.20

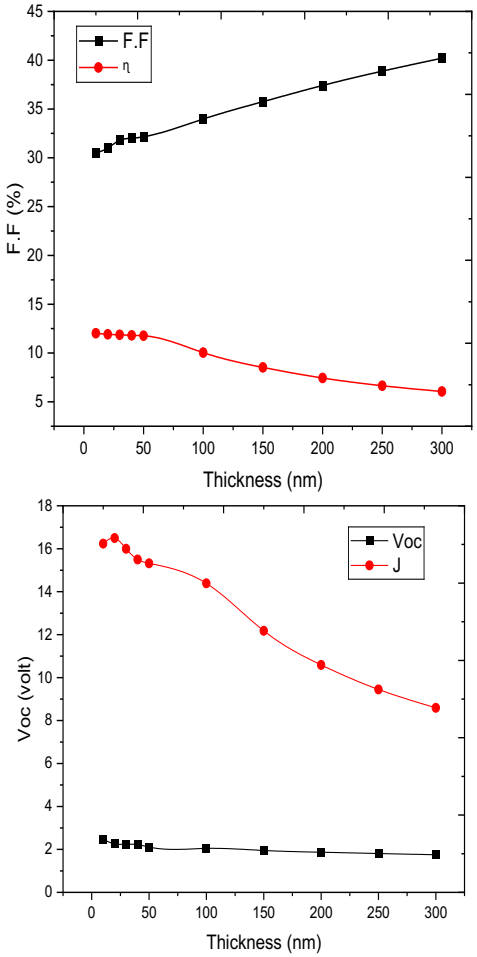

Fig. 2: The variation of V_{oc} (volt), J_{sc} (mA/cm2), FF (%o) and efficiency (%) with the thickness of Gr (nm)

In this study, the impact of the Gr layer thickness on the photovoltaic performance parameters of a solar cell was systematically investigated. The analysis reveals a clear dependence of the open-circuit voltage (V_{oc}), short-circuit current density (Jsc), fill factor (FF), and power conversion efficiency (PCE) on the thickness of the Gr layer.As the

thickness increases from 10 nm to 400 nm, the open-circuit voltage (Voc) shows a gradual decrease from 2.461 V to 1.662 V. This behavior can be attributed to increased recombination losses at higher thicknesses, which hinder the photogenerated charge carriers from reaching the electrodes efficiently.

The short-circuit current density (Jsc) initially increases, reaching its maximum around 100–150 nm, and then decreases as the thickness continues to increase. This indicates that an optimal thickness exists where light absorption is maximized without significantly increasing the recombination losses. The fill factor (FF) demonstrates a consistent increase with thickness, rising from 30.50% at 10 nm to 42.43% at 400 nm. This suggests that thicker Gr layers contribute to improved charge transport and reduced series resistance. Most importantly, the power conversion efficiency (PCE) exhibits a peak value of approximately 7.489% at 200 nm, after which it declines. This clearly indicates that the optimal Gr layer thickness for maximum device performance is approximately 200 nm. Beyond this point, the negative effects on Voc and Jsc outweigh the benefits of the increased FF. Recommendation

To achieve optimal solar cell performance, it is recommended to use a Gr layer thickness around 200 nm. This thickness offers the best compromise between high photocurrent, sufficient voltage, and efficient charge extraction, resulting in maximum device efficiency. [8]

Table 3: Effect of CspbX3 Layer Thickness on Solar Cell Performance Parameters

Thickness(nm) CspbX3	V_{OC} (volt)	J_{SC} $(\frac{mA}{Cm^2})$	F.F (%)	η (%)
250	2.24	16.32	32.16	11.77
300	1.98	16.66	35.57	11.76
350	1.80	16.92	38.24	11.68
400	1.67	17.12	40.42	11.56
450	1.56	17.25	42.34	11.42
500	1.47	17.34	44.06	11.27
550	1.398	17.401	45.59	11.10
600	1.334	17.43	46.92	10.91

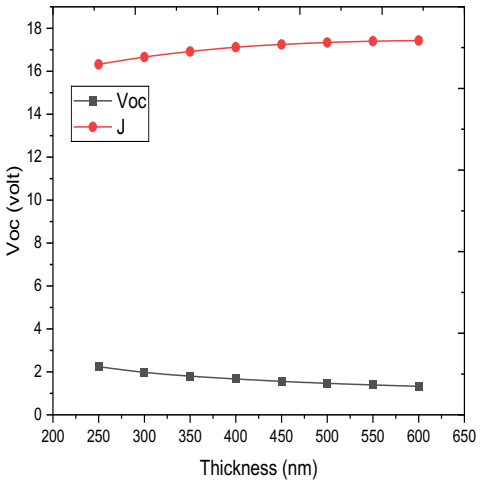

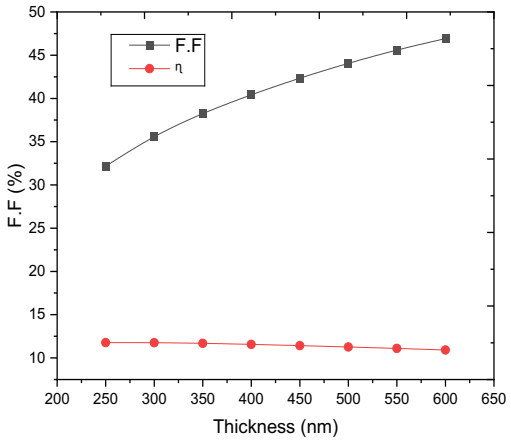

Fig. 3: The variation of Voc (volt), Jsc (mA/cm2), FF (%) and η (%) with the thickness of CspbX3 (nm)

In this study, the effect of the active layer thickness of CsPbX3 on the photovoltaic parameters of the solar cell was investigated, including open-circuit voltage (Voc), short-circuit current density (Jsc), fill factor (FF), and power conversion efficiency (η). The results demonstrated that as the thickness increased from 250 nm to 600 nm, a noticeable decline in the open-circuit voltage was observed, decreasing from 2.24 V to 1.334 V. This reduction can be attributed to increased charge carrier recombination within the thicker active layers, as well as higher internal resistance. In contrast, the short-circuit current density (Jsc) showed a slight improvement, rising from 16.32 mA/cm² to 17.43 mA/cm² with increasing thickness. This behavior is due to enhanced light absorption in thicker films, generating a higher number of charge carriers. Additionally, the fill factor (FF) improved significantly from 32.16% to 46.92%, likely because thicker layers reduce surface defect losses and improve charge collection efficiency at the maximum power point.Despite the increase in Jsc and FF, the overall power conversion efficiency (η) decreased gradually from 11.77% to 10.91% as the thickness increased. This is mainly due to the dominant negative effect of the Voc reduction, which offsets the positive influence of Jsc and FF improvements. In conclusion, the results suggest that thinner active layers, particularly in the range of 250 nm to 350 nm, provide a better balance between high Voc, sufficient Jsc, and a reasonable FF, leading to superior overall device performance. Increasing the thickness beyond this range leads to reduced efficiency, primarily due to increased recombination and resistive losses. [9]

Table 4: Effect of CTN Layer Thickness on Solar Cell Performance Parameters

Thickness(nm) CNT	V_{OC} (volt)	J_{SC} $(\frac{mA}{Cm^2})$	F.F (%)	η (%)
50	2.24	16.235	32.16	11.77
100	2.22	16.610	32.33	11.92
150	2.22	16.76	32.26	12.01
200	2.221	16.84	32.22	12.06

250	2.222	16.87	32.20	12.08
300	2.222	16.88	32.19	12.08
350	2.223	16.89	32.18	12.09
400	2.223	16.89	32.18	12.09

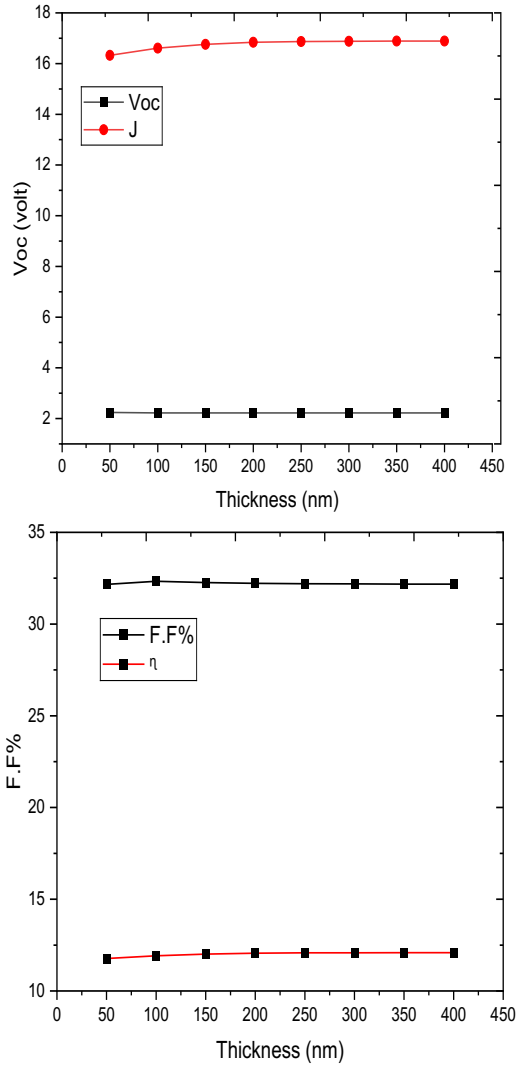

Fig. 4: The variation of Voc (volt), Jsc (mA/cm2), FF (%o) and efficiency (η) with the thickness of CTN (nm)

The obtained results from analyzing the performance of the solar cell with varying CNT layer thicknesses (ranging from 50 to 400 nm) indicate that the thickness significantly influences certain performance parameters, particularly the short-circuit current density (Js c) and overall efficiency. The open-circuit voltage (V_{oc}) remained nearly constant, ranging between 2.22 and 2.24 V, suggesting that the CNT thickness has minimal effect on this parameter. In contrast, the short-circuit current density (J_{sc}) showed a gradual increase with increasing thickness, reaching its maximum at 400 nm. The fill factor (F.F) remained relatively stable across all thickness values, indicating consistent electrical behavior within the cell structure. In terms of efficiency, a noticeable improvement was observed as the CNT layer thickness increased, with the highest efficiency of 12.09% recorded at thicknesses of 350 and 400 nm. This suggests that greater thickness enhances light absorption, thereby improving power conversion.

Therefore, it can be concluded that the optimal CNT layer thickness under the given experimental conditions lies between 350 and 400 nm, where the solar cell achieves its best performance. This study identified the optimal thicknesses for the element layer in solar cells from Gr and CsPbX3 and CNT plants by comparing the photovoltaic performance at different thicknesses. This was achieved by analyzing the effect of thickness on key values such as voltage, voltage, integrated conductance, and scalability, and by optimizing performance under different operating conditions. [10]

Analysis of Solar Cell Performance Using Optimal Layer Thicknesses in SCAPS-1D

Based on the study of how the thickness of individual layers affects the performance of the solar cell, the optimal thickness for each layer—Graphene (Gr), Carbon Nanotube (CNT), and Perovskite—was selected according to the highest recorded efficiency. These values were then used as inputs in SCAPS-1D simulation software to analyze the device's photovoltaic and electrical properties.

Table 5: Selected Optimal Thicknesses

Layer	Optimal Thickness (nm)	Achieved Efficiency (%)
Graphene (Gr)	200	7.489
CNT	350	12.09
Perovskite	250	11.77

These thickness values were applied in a simulated solar cell structure in SCAPS, while other parameters were kept constant. The simulation outputs include:

*Open-circuit voltage (Vos)

*Short-circuit current density (Jsc)

*Fill Factor (FF)

*Power conversion efficiency (η)

Table 6: Simulation Results:

Layer Configuration	V_{OC} (volt)	J_{sc} ($\frac{mA}{Cm^2}$)	F.F (%)	η (%)
Gr (200 nm) + CNT (350 nm) + Perov. (250 nm)	1.8658	10.998	37.31	7.66

Effect of Temperature on Device Performance

To evaluate the thermal stability and overall performance of the optimized solar cell structure, a temperature-dependent simulation was carried out using SCAPS-1D. The device consisted of the previously determined optimal layer thicknesses: Graphene (200 nm), Carbon Nanotube (350

nm), and Perovskite (250 nm). The simulation was conducted over a temperature range of 283 K to 343 K, in steps of 10 K.

The obtained results showed a strong temperature dependence on the solar cell's photovoltaic parameters. As shown in the table below, the open-circuit voltage (Vos) decreased significantly from 2.84 V at 283 K to 0.88 V at 343 K. This drop in Vos is attributed to increased intrinsic carrier concentrations and enhanced recombination rates at higher temperatures.

Meanwhile, the short-circuit current density (Jsc) increased from 9.873 mA/cm² to 13.97 mA/cm², which is likely due to improved photon absorption and carrier generation under elevated thermal conditions. The fill factor (FF) also increased notably, rising from 25.15% to 69.41%, indicating enhanced charge transport and reduced internal resistive losses at higher temperatures. As a result, the overall power conversion efficiency (η) improved from 7.07% at 283 K to 8.61% at 343 K. Despite the reduction in Vos, the gain in Jsc and FF compensated for the loss, leading to an overall improvement in performance. . [11]

Table 7: Temperature Dependence of Solar Cell Performance

Temperature (k)	V_{OC} (volt)	J_{SC} $(\frac{mA}{Cm^2})$	F.F (%)	η (%)
283	2.84	9.87	25.15	7.07
293	2.22	10.51	31.69	7.43
303	1.731	11.21	39.89	7.74
313	1.37	11.92	48.92	8.01
323	1.13	12.64	57.62	8.25
333	0.98	13.32	64.66	8.46
343	0.88	13.97	69.41	8.61

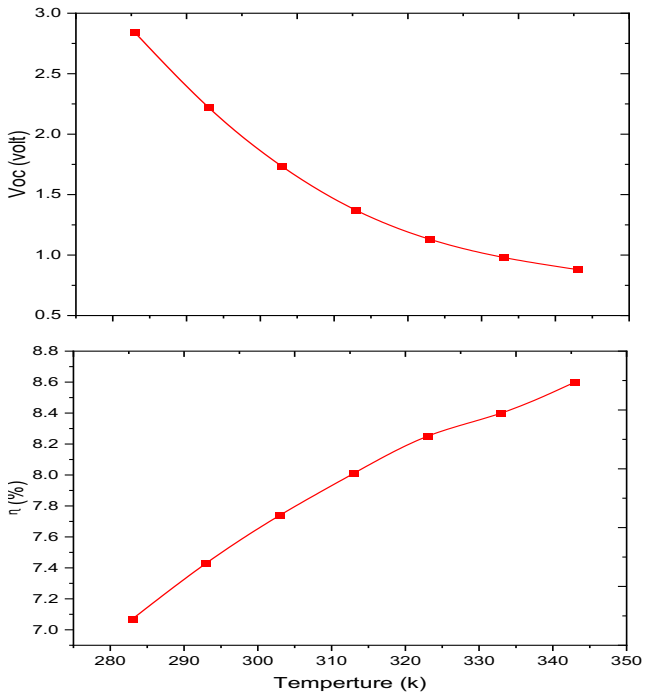

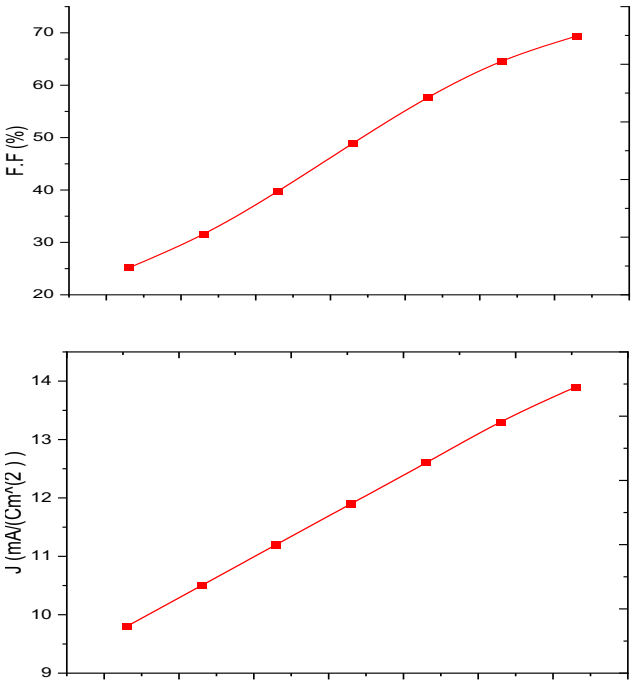

Fig. 7: Effect of Temperature on Voc, Jsc, Fill Factor, and Efficiency of the Solar Cell"

The data indicate that the open-circuit voltage (Voc) decreases significantly with increasing temperature, dropping from 2.84 V at 283 K to 0.88 V at 343 K. This decline can be attributed to the enhanced generation of thermal charge carriers, which increases the recombination rates within the cell and consequently reduces the output voltage.

On the other hand, the results show that the short-circuit current density (Jsc) increases gradually as the temperature rises, from 9.87 to 13.97 mA/cm². This increase is due to the higher concentration of charge carriers generated by the absorption of more photons at elevated thermal energy levels.

Furthermore, it was observed that the fill factor (F.F) improves with increasing temperature, rising from 25.15% to 69.41%. This improvement is linked to the enhanced ability to extract electrical current more efficiently due to reduced internal resistance at higher temperatures. As a result of these combined effects, the overall efficiency (η) of the solar cell increased from 7.07% to 8.61% over the studied temperature range.

Based on these findings, it is evident that temperature has a complex effect on solar cell performance. While it decreases the voltage, it simultaneously enhances both the current and the fill factor, ultimately leading to a positive impact on the overall efficiency. This study highlights the importance of considering thermal effects in the design and operation of photovoltaic systems to achieve optimal performance under various environmental conditions.

The Role of Band Gap in Enhancing the Performance of the Perovskite Layer CSPbX3

The band gap is considered one of the fundamental properties that determine the functional performance efficiency of the perovskite layer $CSPbX_3$ in optoelectronic applications. The value of the band gap directly affects the layer's ability to absorb light and convert it into electrical charges, which in turn impacts the efficiency of devices that depend on it, such as solar cells and lighting devices. Precise control of the band gap in this layer enables a broader absorption of the solar spectrum and better alignment with other device components, thereby contributing to enhanced performance and longer-term stability.

The energy gap depends on the type of halogen X

Typical values for energy balance(approximate) . [12]

Cspbcl3.about3.0 ev

CspbBr3.about2.3 ev

CspbI3.about1.73ev

Table 8: Lightweight perovskite ($CSPbX_3$) layer weight table

Material Formula	Halide Ion (X)	Band Gap (ev)	Notes
CspbCl3	Chloride(Cl-)	~3.0 ev	Suitable for UV detection
CspbBr3	Bromide(Br-)	~2.3 ev	Used in green LEDs And solar cells
CspbI3	Lodide(I-)	~1.73 ev	Suitable for high-efficiency solar cells

Table 9: "Effect of Energy Band Gap on the Performance

Energy band gap (ev) $CsPbCl_3$	V_{OC} (volt)	J_{SC} $(\frac{mA}{Cm^2})$	F.F (%)	η (%)
2.8	2.0	10.5	68.0	5.5
2.9	2.05	9.8	66.5	5.0
3.0	2.1	9.0	65.0	4.5
3.1	2.15	8.2	63.0	4.0
3.2	2.2	7.5	60.0	3.5

Table 10: "Effect of Energy Band Gap on the Performance of $CsPbBr_3$ Solar Cells"

Energy band gap (ev) $CsPbBr_3$	V_{OC} (volt)	J_{SC} $(\frac{mA}{Cm^2})$	F.F (%)	η (%)
2.2	1.6	17.5	70.0	13.0
2.25	1.65	16.8	69.5	12.8
2.3	1.7	16.0	68.0	12.5
2.35	1.75	15.3	66.0	12.0
2.4	1.8	14.5	64.0	11.5

Table 11: "Effect of Energy Band Gap on the Performance of $CsPbI_3$ Solar Cells"

Energy band gap (ev) $CsPbI_3$	V_{OC} (volt	J_{SC} $(\frac{mA}{Cm^2})$	F.F (%)	η (%)
1.6	1.05	26.5	70.0	19.5
1.65	1.1	25.7	71.5	19.8
1.73	1.15	24.9	72.0	19.9
1.75	1.2	24.1	72.5	19.8
1.8	1.25	23.3	71.0	19.5

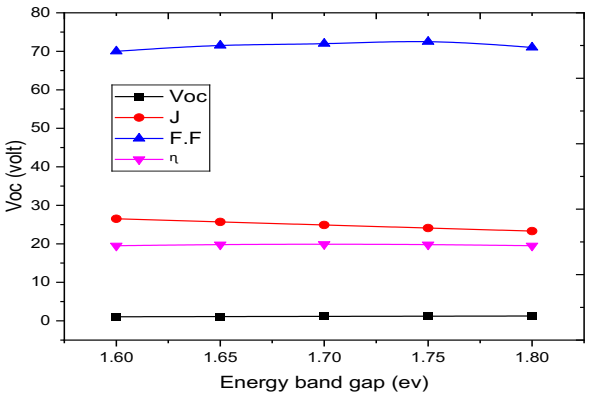

Fig. 11: Characteristics of $CsPbI_3$ Solar Cells at Different Energy Band Gaps"

The results showed that increasing the energy band gap in $CsPbI_3$ solar cells leads to a gradual rise in the open-circuit voltage (Voc) but a decrease in the short-circuit current density (Jsc). Nevertheless, the fill factor (FF) and efficiency (η) remained relatively stable. It can be concluded that an energy band gap between 1.7 and 1.75 eV offers an optimal balance for cell performance.

Table 12: Influence of CNT Energy Band Gap on Photovoltaic Performance Parameters (Voc, Jsc, FF, η)

Energy band gap CNT	V_{OC} (volt)	J_{SC} $(\frac{mA}{Cm^2})$	F.F (%)	η (%)
0.2	0.65	32.5	66.0	15.8
0.25	0.68	31.8	67.5	16.2
0.3	0.70	31.0	68.0	16.4
0.35	0.73	30.3	68.5	16.6
0.4	0.76	29.7	69.0	16.8

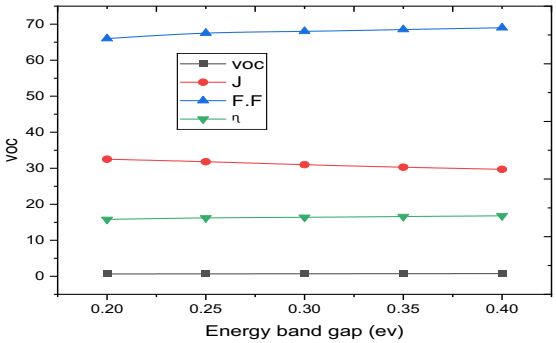

Fig. 12: Variation of Voc, Jsc, FF, and Efficiency with CNT Energy Band Gap"

It was found that increasing the energy band gap (Band Gap) from 0.2 to 0.4 eV leads to:

An increase in open-circuit voltage (Voc) from 0.65 V to 0.76 V.A decrease in short-circuit current density (Jsc) from 32.5 to 29.7 mA/cm².An improvement in fill factor (FF) from 66.0% to 69.0%.An increase in efficiency (η) from 15.8% to 16.8%.It is concluded that an energy band gap between 1.7 and 1.75 eV provides an optimal balance for CNT-based solar cell performance. [15]

Table 13: Effect of Graphene Energy Band Gap on Photovoltaic Parameters (V_{oc}, J_{sc}, FF, η) of Solar Cell

Energy band gap Gr	V_{OC} (volt	J_{sc} $(\frac{mA}{Cm^2})$	F.F (%)	η (%)
0.1	0.02	30.00	25.00	0.15
0.2	0.04	29.80	30.00	0.36
0.3	0.06	29.60	35.00	0.62
0.4	0.09	29.30	40.00	1.05
0.5	0.11	29.00	45.00	1.44

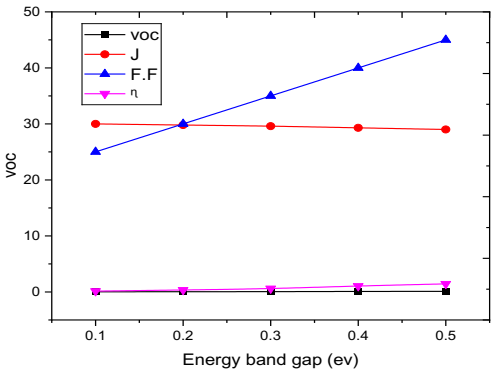

Fig. 13: Effect of energy gap on Voc, Jsc, FF and efficiency

The results showed that increasing the energy band gap leads to an increase in the open-circuit voltage (V_{oc}), fill factor (FF), and cell efficiency (η), while the short-circuit current density (J_{sc}) slightly decreases. Overall, increasing the energy band gap improves the overall performance of the solar cell within the studied range.

3 Conclusions

In this study, the SCAPS-1D software was utilized to simulate the performance of a GR/CNT-based solar cell. The results indicate that increasing the thickness of the CNT layer contributes positively to the device's efficiency, while increasing the thickness of the GR layer may lead to a decline in performance due to its impact on optical or electrical properties. The GR/CNT solar cell achieved a power conversion efficiency of 7.66%, highlighting its potential as a promising candidate for solar energy conversion. The simulation results emphasize the effective role of carbon nanotubes in enhancing solar cell performance, supporting their potential use in future photovoltaic applications.

References

[1] S. M. Iftiquar and J. Yi, "Numerical simulation and light trapping in perovskite solar cell," Journal of Photonics for Energy, vol. 6, no. 2, Article ID 025507, 2016.

[2] M. H. Mohammadi, D. Fathi, and M. Eskandari, "NiO@GeSe core–shell nano-rod array as a new hole transfer layer in perovskite solar cells: A simulation study," Solar Energy, vol. 211, pp. 522–525, 2020.

[3] S. Rani, A. Kumar, and D. S. Ghosh, "Optical designing of perovskite solar cells," IEEE Journal of Photovoltaics, vol. 12, no. 2, pp. 595–601, 2022, doi: 10.1109/JPHOTOV.2021.3139306.

[4] Liu, M., Johnston, M. B., & Snaith, H. J. (2014). Efficient planar heterojunction perovskite solar cells by vapor deposition. Nature, 501, 395–398.

[5] Minemoto, T., & Murata, M. (2014). Device modeling of perovskite solar cells based on structural similarity with thin film inorganic semiconductor solar cells. Japanese Journal of Applied Physics, 53(4S), 04ER05.

[6] Gong, J., Darling, S. B., & You, F. (2015). Perovskite photovoltaics: Life-cycle assessment of energy and environmental impacts. Energy & Environmental Science, 8(7), 1953–1968.

[7] Zhou, H., Chen, Q., Li, G., Luo, S., Song, T.-B., Duan, H.-S., Hong, Z., You, J., Liu, Y., & Yang, Y. (2016). Interface engineering of highly efficient perovskite solar cells. Science, 345(6196), 542–546.

[8] Rehman, M. A., Roy, S. B., Akhtar, I., Bhopal, M. F., Choi, W., Nazir, G., Khan, M. F., Kumar, S., Eom, J., Chun, S.-H., & Seo, Y. (2019). Thickness-dependent efficiency of directly grown graphene based solar cells. Carbon, 148, 187–195. https://doi.org/10.1016/j.carbon.2019.03.079

[9] Son, H., & Jeong, B.-S. (2022). Optimization of the Power Conversion Efficiency of $CsPbIxBr_{3-x}$-Based Perovskite Photovoltaic Solar Cells Using ZnO and NiOx as an Inorganic Charge Transport Layer. Applied Sciences, 12(18), 8987.

[10] S. A. Britz, D. M. Bagnall, and J. R. Durrant, "Replacement of Transparent Conductive Oxides by Single-Wall Carbon Nanotubes in $Cu(In,Ga)Se_2$-Based Solar Cells," Journal of Physical Chemistry C, vol. 115, no. 40, pp. 19993–19998, 2011.

[11] Ukwenya, J. A., Owolabi, J. A., Onimisi, M. Y., Danladi, E., Udeh, S. M., & Ushiekpan, U. R. (2023) The Effect of Temperature Dependence on Tin Perovskite Solar Cell Using SCAPS-1D. FU DMA Journal of Sciences (FJS), 7(2). https://fjs.fudutsinma.edu.ng/index.php/fjs/article/view/2044

[12] Nie, W., Tsai, H., Asadpour, R., Huang, J., & others. (2018). $CsPbX_3$ perovskites for efficient and stable photovoltaics. Joule, 2(10), 1610–1623. https://doi.org/10.1016/j.joule.2018.06.007

[13] Shen, L., Yang, Y., Liu, H., et al. (2022). Performance enhancement of $CsPbI_3$ perovskite solar cells by optimizing energy band gap. Solar Energy Materials and Solar Cells, 243, 111771. https://doi.org/10.1016/j.solmat.2022.111771

[14] Zhao, Q., Wang, J., Zhang, W., et al. (2020). Perovskite $CsPbI_3$ solar cells with improved stability and performance. eScholarship, University of California. https://escholarship.org/uc/item/57q6105f

[15] Monocrystalline 1.7-eV-Bandgap MgCdTe Solar Cell With 11.2% Efficiency: Monocrystalline 1.7-eV-Bandgap MgCdTe Solar Cell With 11.2% Efficiency: Journal of Electronic Materials: https://www.osti.gov/servlets/purl/1579873

[16] AbdulAlmohsin, S. M. (2021). Hybrid Structure Organic / Inorganic Perovskites Solar Cells (Master's thesis). University of Thi-Qar. Retrieved April 15, 2025, from https://dspace.utq.edu.iq/handle/123456789/393

[17] AbdulAlmohsin, S. M. (2021). Study and Preparation of Solid State Dye Sensitized Solar Cell using D149 as a Dye, TiO_2 Nanoparticles as a Photo-anode and MWCNTs as a Counter Electrode (Master's thesis). Iraqi Digital Repository. Retrieved April 15, 2025, from https://iqdr.iq/search?view=d40dbb6ef271c1807d3594132b8453e5

[18] Abdulsada, Z. R., & Abdula Mohsin, S. M. (2021). High Efficiency Solar Cells Base on Organic-inorganic Perovskites Materials. University of Thi-Qar Journal of Science, 8(2), 23–29. https://doi.org/10.32792/utq/utjsci.v8i2.808

[19] Edam, M. J., Khadier, H. M., & AbdulAlmohsin, S. M. (2024). Highest Efficiency of Perovskite Structure Solar Cells. International Journal of Thin Film Science and Technology, 13(1). http://dx.doi.org/10.18576/ijtfst/130105

[20] Rashash, H. A. (2024). Optimization of Temperature, Defects, and Thickness for High Efficiency of Tin Halide Perovskites. ResearchGate. Retrieved April 15, 2025, from https://www.researchgate.net/publication/381098101_Optimization_of_Temperature_Defects_and_Thickness_for_High_Efficiency_of_Tin_Halide_Perovskites

[21] Rashash, H. A. (2023). (Master's thesis defense announcement). Technical Institute Al-Samawa, University of Thi-Qar. Retrieved April 15, 2025, from https://isa.atu.edu.iq/?p=15298

[22] Swiechowicz, Kasielska-Trojan, A., Manning, J. f- and Antozewski, B. (2022). Can Digit Ratio (2D:4D) Be Indicative of Predispositions to Autoimmune Thyroid Diseases in Women Hashimoto Thyroiditis and Graves ' Disease ?. Frontiers in endocrinology, 13, Pp:914471

[23] Wen, W., and Liu, F. (2007). Autoantibodies highly increased in patients with hyroid dysfunction. Cell. Molec. Immunol, 4(3), pp:233-236.

[24] Mondal, S. I, Das, S. A., Akter, A, Hasan, R., Talukdar, S. A., And Reza, M. S. (2011). Thyroid hormone and its correlation with age, sex and serum lipid levels in hypothyroid andeuthyroid sylheti populations in Bangladesh. Young, 25, pp:40,

[25] Peterson, G. (2011). Subclinical hypothyroidism in the elderly: a common dilemma. Australian Pharmacist, 30(7), pp:555-556.

[26] Stagnaro-Green, A., Abalovich, M., Alexander, E, Azizi, F, Mestman, J, Negro, R., and Wiersinga, W. (2011). American Thyroid Association Taskforce on Thyroid Disease During Pregnancy and Postpartum. Guidelines of the American Thyroid Association for the diagnosis and management of thyroid disease during pregnancy and postpartum. Thyroid, 21(10), pp:1081-1125.

[27] Ferari, S. M. Fallahi, P., Rufl, I, Elia, G., Ragusa,F., Benvenga, S, and Antonelli, A. The association of other autoimmune diseases in patients with Graves" disease (with or without ophthalmopathy): review of the literature and report of a large series. Autoimmunity reviews, 18/(3), pp:287-292.

[28] Prepare heterostructure of MoS2/TiO2 solar cell via simple two-steps by hydrothermal method Basrah University, College science, Physics Department, Basrah University, College science, Physics Department. 2023-11-04

[29] Solar cell with double quantum dot structure Amin Habbeb Al-Khursan , Suha Hadi, 262-280, 2020-12-03

[30] Optimization of Temperature, Defects, and Thickness for High Efficiency of Tin Halide Perovskites Hussein.A. Rshash, Samir M. Abdul Almohsin, 2024-06-01